Luminescent Photofragments of (1,1,1,5,5,5-Hexafluoro-2,4-pentanedionato) Metal Complexes in the Gas Phase

David S. Talaga, Stephen D. Hanna, and Jeffrey I. Zink*

Department of Chemisty and Biochemistry, University of California, Los Angeles, Los Angeles, California 90095-1569

Received October 22, 1997

The luminescence that is observed under gas phase photolytic deposition conditions is studied for $Cr(hfac)_3$, $Ni(hfac)_2$, and $Pt(hfac)_2$. This luminescence is analyzed under a variety of conditions, including the relatively high pressures of an evacuated gas cell and the collision-free conditions of a molecular beam. The effects of inert buffer gas are also studied. Features in these spectra indicate that, in general, multiple photolysis processes occur. Some simple fragments that are produced from these compounds are identified, including bare metal atoms (Ni, Cr), metal monofluorides (NiF, CrF), CH (in the case of $Ni(hfac)_2$), and metal carbide from $Pt(hfac)_2$. It is postulated that the difference in the observed photofragmentation pathway in the case of platinum is due to σ bonding to the β carbon of the hfac moiety as opposed to the bidentate bonding of the other two metals. Possible mechanisms are presented. Detailed analysis of the spectra allows characterization of the internal energy of the platinum carbide photofragment.

Introduction

Recent studies have shown that luminescence is observed when metal-containing molecules are irradiated under photochemically driven chemical vapor deposition (CVD) conditions and that luminescence spectroscopy can be used to identify photofragments and assist in the elucidation of the photolytic deposition pathways.[1−3] Laser-assisted metal organic CVD relies on the use of volatile organometallic compounds to deliver material to a substrate where the compound is photodecomposed leaving behind the material to be deposited (and possibly undesired contaminants).[2−14] Laser-assisted CVD has the advantages of spatially selective deposition on the substrate, selective energy transfer to the deposition precursor, and low processing temperature.[15−21] Efforts to fabricate multilayer structures with well-defined physical properties and abrupt interfaces benefit from the low growth temperatures.[22−24]

Metal acetylacetonate (2,4-pentanedionate = acac) complexes have found utility as CVD precursors[25−27] including applications in metallization for semiconductor interconnects[17] and preparation of metal oxides for high T_c superconducting films.[28] Fluorinated acetylacetonate Iigands (1,1,1,5,5,5-hexafluoro-2,4-pentanedionate = hfac) increase sample volatility and allow for more facile transport in the gas phase but may result in fluorine contamination of the final deposit.[29] For example, photolytic CVD of copper from $Cu(hfac)_2$ shows measurable fluorine incorporation.[30,31] Luminescence spectra were used to identify the photofragments resulting from photolysis of $Cu(hfac)_2$ in the gas phase.[1] The luminescence from 308 nm excitation of $Cu(hfac)_2$ under "high pressure" conditions (∼1 bar), "low pressure" conditions (∼0.1−10 mbar), and collision-free conditions (molecular beam, 10^{-4} mbar) was studied to provide

(1) Talaga, D. S.; Zink, J. I. *Inorg. Chem.* **1996**, *35*, 5050.
(2) Wexler, D.; Zink, J. I.; Tutt, L. W.; Lunt, S. R. *J. Phys. Chem.* **1993**, *97*, 13563.
(3) Cheon, J.; Talaga, D. S.; Zink, J. I. *J. Am. Chem. Soc.* **1997**, *119*, 163.
(4) Cheon, J.; Talaga, D. S.; Zink, J. I. *Chem. Mater.* **1997**, *9*, 1208.
(5) Cheon, J.; Zink, J. I. *J. Am. Chem. Soc.* **1997**, *119*, 3838.
(6) Mogyorosi, P.; Carlsson, J. O.; Moradi, M. *Appl. Surf. Sci.* **1992**, *54*, 46.
(7) Messelhauser, J.; Flint, E. B.; Suhr, H. *Appl. Surf. Sci.* **1992**, *54*,64.
(8) Vogel Koplitz, L.; Shuh, D. K.; Chen, Y. J.; Williams, R. S.; Zink, J. I. *Appl. Phys. Lett.* **1988**, *53*, 1705.
(9) Rand, M. J. *J. Electrochem. Soc.* **1973**, *120*, 686.
(10) Cohan, J. S.; Yuan, H.; Williams, R. S.; Zink, J. I. *Appl. Phys. Lett.* **1992**, *60*, 1402.
(11) Flint, E. B.; Messelhauser, J.; Suhr, H. *Appl. Phys. A* **1991**, *53*, 430.
(12) Kargl, P. B.; Kullmer, R.; Bauerle, D. *Appl. Phys. A* **1993**, *57*, 175.
(13) Mogyorosi, P.; Carlsson, J. O. *Mater. Res. Soc. Symp. Proc.* **1992**, *236*,123.
(14) (a) Heszler, P.; Carlsson, J. O.; Mogyorosi, P. *J. Vac. Sci. Technol. A* **1993**, *11*, 2924. (b) Hester, P.; Mogyorosi, P.; Carlsson, J. O. *Appl. Surf. Sci.* **1993**, *69*, 272. (c) Heszler, P.; Mogyorosi, P.; Carlsson, J. O. *Appl. Surf. Sci.* **1993**, *69*, 376. (d) Heszler, P.; Mogyorosi, P.; Carlsson, J. O. *J. Appl. Phys.* **1995**, *78*, 5277.
(15) Avey, A. A.; Hill, R. H. *J. Am. Chem. Soc.* **1996**, *118*, 237.
(16) Larciprete, R. *Appl. Surf. Sci.* **1990**, *46*, 19.
(17) Doppelt, P.; Baum, T. H. *Mater. Res. Soc. Bull.* **1994**, *19*, 41.
(18) Lee, E. J. B.; Bitner, T. W.; Ha, J. S.; Shane, M. J.; Sailor, H. J. *J. Am. Chem. Soc.* **1996**, *118*, 5375.
(19) Bhatia, S. K.; Hickman, J. J.; Ligler, F. S. *J. Am. Chem. Soc.* **1992**, *114*, 4432.
(20) Dressick, W. J.; Dulcey, C. S.; Georger, J. H.; Calvert, J. M. *Chem. Mater.* **1993**, *5*, 148.
(21) Moreau, W. M. *Semiconductor Lithography; Principles, Practices, and Materials*; Plenum: New York, 1988.
(22) Kompa, K. L. *Angew. Chem., Int. Ed. Engl.* **1988**, *27*, 1314.
(23) Herman, I. P. *Chem. Rev.* **1989**, *89*, 1323.
(24) Eden, J. G. *Photochemical Vapor Deposition*; Wiley: New York, 1992.
(25) Hitchman, M. L.; Jensen, K F. *Chemical Vapor Deposition: Principles and Applications*; Academic Press: San Diego, 1993.
(26) Kodas, T. T.; Hampden-Smith, M. J. *The Chemistry of Metal CVD*; VCH: Weinheim, 1994.
(27) Kaesz, H. D.; Williams, R. S.; Hicks, R. F.; Zink, J. I.; Chen, Y. J.; Muller, H. J.; Xue, Z. L.; Xu, D. Q.; Shuh, D. K.; Kim, Y. K. *New J. Chem.* **1990**, *14*, 527.
(28) Schulz, D. L.; Marks, T. J. *Adv. Mater.* **1994**, *6*, 719.
(29) Nemoto, M.; Yamanaka, M. *J. Mater. Res.* **1990**, *5*, 1.
(30) Jones, C. R.; Houle, F. A.; Kovac, C. A.; Baum, T. H. *Appl. Phys. Lett.* **1985**, *46*, 97.
(31) Houle, F. A.; Wilson, R. J.; Baum, T. H. *J. Vac. Sci. Technol. A* **1986**, *4*, 2452.

S0020-1669(97)01340-2 CCC: $15.00
Published on Web 06/15/1998

information about the photofragmentation process and the role of molecular collisions in photofragmentation to form metal deposits. Surprisingly, under collision-free conditions only CuF luminescence was observed. One goal of the present study is to determine if metal fluorides are a common photoproduct resulting from photolysis of metal hexafluoroacetylacetonate complexes. An obstacle in determining the generality of photolytic diatomic metal fluoride production from metal hexafluoroacetylacetonates is the general paucity of spectroscopic data available on the diatomic metal fluorides. For a definitive assignment of an observed luminescence band to a metal fluoride (or any other species for that matter), it is helpful to use known spectroscopic band assignments. In our original study of $Cu(hfac)_2$ we used the detailed spectroscopic analyses of the various band systems of CuF. Unfortunately there are very few metal fluorides for which this level of detail is known. Many electronic states of nickel fluoride have been assigned in the literature.[32] Because of this and because of nickel's proximity to copper in the periodic table, we chose to investigate the photofragmentation of $Ni(hfac)_2$. Similarly, CrF has been spectroscopically characterized in the literature[33−35] allowing the possibility of definitive identification of this species if it is a photoproduct of $Cr(hfac)_3$. $Cr(hfac)_3$ is also studied to investigate the differences, if any, in the gas phase photodecomposition under deposition conditions between metal bis- and trishexafluoroacetylacetonate species. $Cr(hfac)_3$ is six-coordinate based on an octahedral coordination structure, whereas $Cu(hfac)_2$ and $Ni(hfac)_2$ are four-coordinate planar complexes.

In our prior work on $Cu(hfac)_2$ we proposed two mechanisms by which metal fluoride production could occur; one was based on metal binding to the hfac through the β carbon. Because this type of bonding has been shown to exist in $Pt(hfac)_2$ this molecule is studied to investigate the possible contribution of Pt−C bonding to the fragmentation mechanism and its possible importance in platinum CVD. Platinum films grown from the unfluorinated $Pt(acac)_2$ precursor exhibit large amounts of carbon contamination.[8,9]

In this paper, the luminescence that is observed under gas phase photolytic deposition conditions is studied for Cr, Ni, and Pt hfac compounds. This luminescence is analyzed under a variety of conditions, including the relatively wide range of pressures available in an evacuated gas cell and the collision-free conditions of a molecular beam. The effects of inert buffer gas are also studied. Features in these spectra indicate that, in general, multiple photolysis processes occur. We identify some simple fragments that are produced from these compounds and discuss the differences and similarities between the compounds studied. Detailed analysis of the spectra allows characterization of the internal energies of the fragments to be determined. We provide this level of analysis for the platinum photofragments.

Experimental Procedures

Spectroscopic Techniques. The light source for the spectroscopic investigations is a Lambda Physik EMG 201 MSC XeCl excimer laser coupled with a Lambda Physik FL2001 excimer-pumped dye laser operating with coumarin 440 or *p*-terphenyl as the dye. The pulse width is 12 ns. The 308 nm pulse energy used for excitation of the CVD precursors is varied from approximately 0.3 to 30 mJ. The dye laser pulse energy was typically 2 mJ for 343 nm and 4 mJ for 440 nm.

Luminescence spectra under deposition conditions are measured in a continuously evacuated glass spectroscopy cell fitted with quartz windows. A sample of the CVD precursor is placed in the sample chamber and is leaked into the photolysis chamber with a Teflon valve. Buffer gases are introduced via a separate inlet. Alternatively, an evacuated stainless steel six-way cross with synthetic fused silica windows is used. A sample of the CVD precursor is placed in the sample chamber and is leaked into the photolysis chamber with a needle valve. Buffer gases can be introduced in conjunction with the sample or via a separate inlet allowing luminescence spectra to be obtained under a variety of pressure conditions [e.g. dynamic vacuum (10^{-2} Torr), static vacuum, Ar buffer gas (∼1−1000 Torr)]. For both chambers, the entire cell is heated to the sublimation temperature of the compound studied (typically 70−140 °C) using thermostated heating tape. Both of these chambers are referred to as the "gas cell" in the text.

The laser is focused with a $\varnothing = 1$ in., $f = 50$ mm, quartz lens. The resulting fluence is typically ∼3 MW/cm^2 for the excimer and ∼12 MW/cm^2 for the dye laser. The focused output of a XeCl excimer laser (308 nm), or an excimer pumped dye laser (343 or 440 nm) excites the gaseous sample and the emitted light is collected by *f*/4 optics at right angles and directed into a 0.32 m single monochromator (JY HR320) where it is dispersed by a 300 or 600 gr/mm holographic grating and detected by an UV-intensified diode array detector (EG&G Princeton Applied Research OMA3, 1024 × 1) or a liquid nitrogen cooled CCD detector (Princeton Instruments, 1024 × 256). The spectral width of a pixel is ∼0.24 and ∼0.12 nm for the 300 and 600 gr/mm gratings, respectively. The UV intensifier allows time-resolved gating of the detector with a resolution of 10 ns.

The molecular beam experiments are carried out in a cubic stainless steel vacuum chamber (30 cm edge length). A mechanical pump and a directly connected 12 in. diffusion pump are used to evacuate the chamber. Background pressures of 6×10^{-5} and 5×10^{-6} torr are typical of operation with and without the molecular beam, respectively. The seeded carrier gas (Ar or He at 50−1000 mbar stagnation pressure) expands continuously through a ∼100 μm pinhole into the chamber. The laser is focused with a $\varnothing = 1$ in., $f = 1000$ mm, quartz lens. The resulting fluence is typically ∼8 MW/cm^2 for the excimer and ∼2 MW/cm^2 for the dye laser. The molecular beam is intersected by the focused output of the laser 1.5 cm downstream. The light is collected by *f*/5 optics and directed into a 0.67 m single monochromator, where it is dispersed by a 600 gr/mm or a 1800 gr/mm holographic grating and detected by a liquid nitrogen cooled CCD detector (Princeton Instruments, 1024 × 256). The spectral width of a pixel is ∼0.066 and ∼0.019 nm for the 600 and 1800 gr/mm gratings, respectively. Spectra were calibrated externally by taking standard neon and mercury spectra assuming linear dispersion of wavelength over the spectral region. Spectra were more accurately calibrated in cases where known atomic lines appeared.

Materials. Chromium hexafluoroacetylacetonate, nickel hexafluoroacetylacetonate, and platinum hexafluoroacetylacetonate were obtained from Strem Chemical Company and used either without further purification or following sublimation. Sublimation of the compounds did not change the spectra observed.

Results

1. $Ni(hfac)_2$. Low-Pressure Gas Phase Luminescence. Under 308 nm excitation and low-pressure conditions (pressure less than or equal to the vapor pressure of the compound), the spectrum in Figure 1a is observed. There are a multitude of sharp peaks between 340 and 400 nm with additional sharp peaks at 538.7, 542.1, and 547.4 nm. These peaks have a short lifetime as illustrated in the short-time gated spectrum in Figure 1b. This spectrum is acquired with the high-voltage gate on for 10 ns during the laser shot. Longer delay times result in the spectrum that appears in Figure 1c. This spectrum is acquired by delaying the gate for 100 ns and turning it on for 100 μs thereafter, thereby reducing the contributions from short-lived species. These longer lived peaks, which are broader, are

(32) Dufour, C.; Hikmet, I.; Pinchemel, B. *J. Mol. Spectrosc.* **1994**, *165*, 398.
(33) Dubov, V. M.; Shenyavskaya, E. A. *Opt. Spektrosk.* **1987**, *62*, 326.
(34) Launila, O. *J. Mol. Spectrosc.* **1995**, *169*, 373.
(35) Devore, T. C.; McQuaid, M.; Gole, J. L. *High Temp. Sci.* **1990**, *29*, 1.

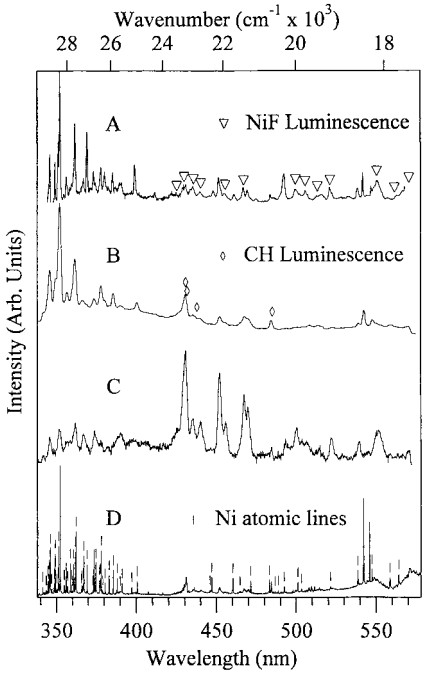

Figure 1. Emission spectra observed from 308 nm excitation of Ni(hfac)$_2$ in the gas phase. (a) Spectrum observed at a pressure of no greater than the vapor pressure of Ni(hfac)$_2$. The triangles mark the wavelengths of known NiF transitions as summarized in Table 2. (b) Low-pressure gas cell spectrum of Ni(hfac)$_2$ showing the components which have a short (~10 ns) lifetime. The diamonds mark luminescence due to CH. (c) Low-pressure gas cell spectrum of Ni(hfac)$_2$ showing the components which have a long (>100 ns) lifetime. Note the relative enhancement of the NiF bands. (d) Emission spectra arising from 308 nm excitation of Ni(hfac)$_2$ in a molecular beam of Ni(hfac)$_2$ seeded in argon. The short verticle lines mark the wavelengths of Ni atomic emission. Prominent Ni atomic lines are observed at 346.14, 352.41, 362.43, 542.38, and 546.07 nm.

observable at 425.0, 429.2, 435.2, 439.9, 451.6, 455.1, 467.1, 499.8, 506.0, 513.2, 521.1, 551.0, 563.2, and 571.1 nm. Additional peaks are present at 371.0, 371.7, 387.1, 389.9, 399.1, 411.5, 422.2, 445.7, 448.1, 452.8, 461.2, 469.5, 475.0, 483.8, 486.1, 516.0, 532.8, 544.6, and 545.1 nm.

Collision-Free Luminescence from a Molecular Beam. Under the collision-free conditions of the molecular beam and 308 nm excitation the spectral features present under the low-pressure conditions resolve into distinct structured bands (Figure 1d). These spectra were acquired using the 600 gr/mm grating. The sharp bands between 340 and 400 nm resolve further into a multitude of bands each with a fwhm of approximately 10 cm^{-1} with some weaker broad bands underneath them at 371.0, 371.7, 387.1, 389.9, and 399.1 nm. The band system at 431 nm resolves into a series of rotational lines with a spacing of ~28 cm^{-1} and band heads. The bands at 425.0, 429.2, 435.2, 439.9, 451.6, 455.1, 467.1, 499.8, 506.0, 513.2, 521.1, 551.0, 563.2, and 571.1 nm are present but remain unstructured. The additional resolution and reduction in background allows observation of additional bands at 365.71, 366.14, 366.90, 373.02, 377.23, 377.76, 379.19, 385.80, 388.15, 391.25, 397.12, 400.55, 447.03, 460.44, 471.52, 501.12, 503.36, 506.49, 507.97, 509.54, 511.40, 514.52, 546.07, 558.75, and 564.19 nm.

2. Cr(hfac)$_3$. Low-Pressure Gas Phase Luminescence. Figure 2a and b displays the luminescence spectra obtained from the low-pressure gas cell. The spectra from the chromium compound are substantially richer in features than those from the nickel and platinum compounds. All features are observed under both 308 nm excitation and 343 nm excitation. Under

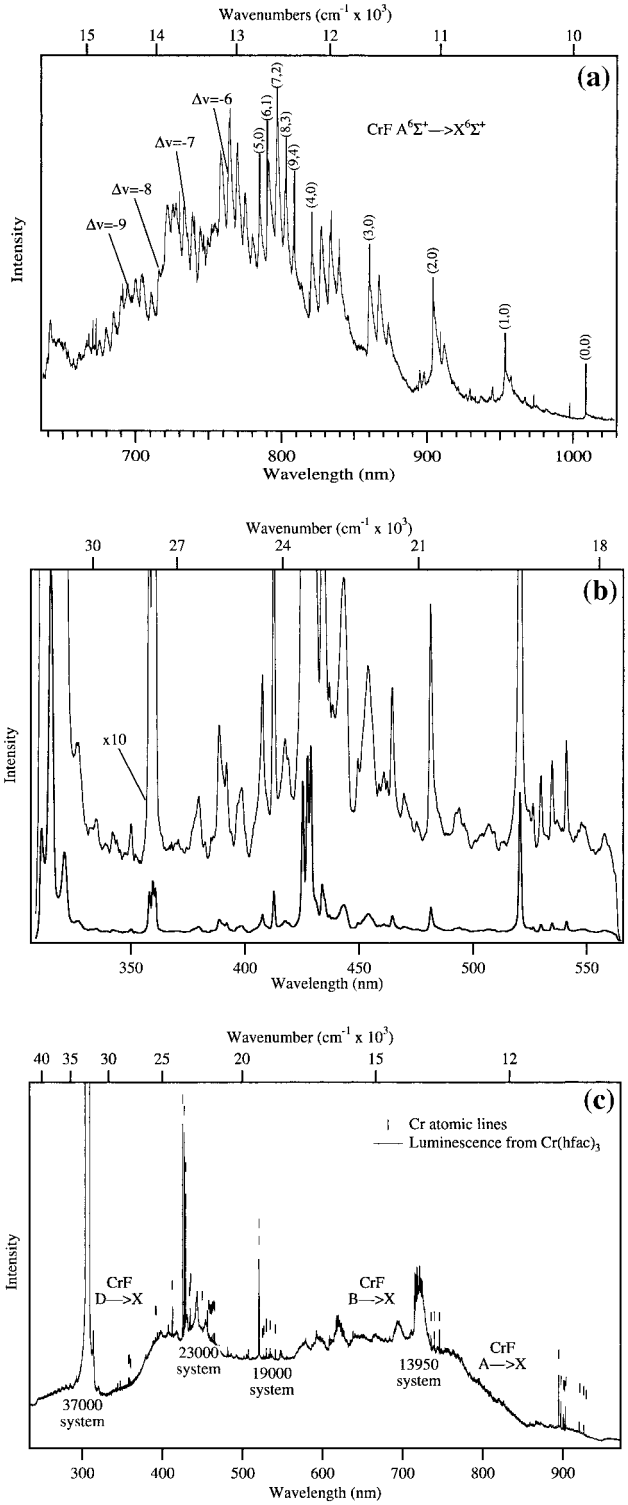

Figure 2. (a) Low-pressure gas cell spectrum of Cr(hfac)$_3$ showing spectral features in the red and near-infrared. Assignments of the vibronic transitions observed for the CrF $A^6\Sigma \rightarrow X^6\Sigma$ system are shown. The $\Delta v = -5$ cluster is assigned in detail. Further details of the assignments are in the text and in Table 1. (b) Low-pressure gas cell spectrum of Cr(hfac)$_3$ showing spectral features in the visible. The top trace is 10× expansion of the lower trace to show details in the baseline. (c) Dispersed luminescence from Cr(hfac)$_3$ excited at 308 nm in a molecular beam. Cr atomic lines are marked with short vertical lines. Prominent Cr atomic lines are observed at 425.43, 427.48, 428.97, 520.45, 520.60, 520.84, 740.02, 746.24, and 894.73 nm. Various band systems are indicated and are described in more detail in the text.

343 nm excitation, some features are more pronounced and better signal to noise is achieved (see below).

Table 1. Observed Peaks from CrF $A^6\Sigma \rightarrow X^6\Sigma$ Band Emission and Their Assignments[a]

assignment (v,v')	observed (cm^{-1})	reported[34] (cm^{-1})
(10,1)	14813	
(11,2)	14716	
(12,3)	14605	
(13,4)	14494	
(14,5)	14398	
(9,1)	14292	
(10,2)	14201	
(11,3)	14076	
(12,4)	13972	
(8,1)	13746	
(9,2)	13642	
(10,3)	13540	
(11,4)	13442	
(7,1)	13192	
(8,2)	13082	
(9,3)	12997	
(10,4)	12821	
(11,5)	12906	
(5,0)	12745	12762.9
(6,1)	12646	12663.9
(7,2)	12546	
(8,3)	12460	
(9,4)	12375	
(10,5)	12297	
(4,0)	12187	12201.9
(5,1)	12093	
(6,2)	12002	
(7,3)	11918	
(8,4)	11829	
(3,0)	11628	11635
(4,1)	11539	11545.7
(5,2)	11455	
(2,0)	11060	11064
(3,1)	10976	10979.3
(1,0)	10490	10490.4
(0,0)	9912	9915.8

[a] The literature values for the band edges of identically assigned peaks are also given.

In the red and near-infrared regions of the emission spectrum, a broad vibronic feature is observed (see Figure 2a). This feature is observed under both 343 and 308 nm excitation, with the best signal to noise ratio obtained under 343 nm excitation. This band system is centered at approximately 13 000 cm^{-1} and is highly structured. The peaks are clustered into well-defined groups. The spacing between each group of peaks is approximately 585 cm^{-1}, while the spacing between individual adjacent peaks ranges from 85 to 125 cm^{-1}. There are at least five well-defined groupings of peaks. This band system extends from 15 500 to 10 000 cm^{-1}. Toward higher energy the bands become obscured due to spectral congestion. The dominant features of this band system are listed in Table 1.

In the visible region of the spectrum (25 000−16 000 cm^{-1}) many intense sharp (fwhm = 10 cm^{-1}) line features are observed as a result of 308 nm photolysis (see Figure 2b). In addition there are many broader features observed at 23 154, 22 498, and 21 814 cm^{-1}. These broader features are obscured by the sharp line features.

At energies higher than the 308 nm laser excitation source, a long regular vibronic progression centered at 37 000 cm^{-1}, is observed. The band consists of eight vibronic features but is obscured to lower energy by the presence of the laser line. The spacing between features is approximately 650 cm^{-1}. The bands have an average fwhm of approximately 300 cm^{-1}. Features are observed between 35 000 and 40 000 cm^{-1}. This band system was observed with the monochromator in second order using the appropriate cutoff filters.

Collision-Free Luminescence from a Molecular Beam. Figure 2c shows the luminescence spectrum observed from Cr-$(hfac)_3$ in a molecular beam under 308 nm excitation. All of the features observed under deposition conditions (discussed above) are also observed in the molecular beam, but many new features appear.

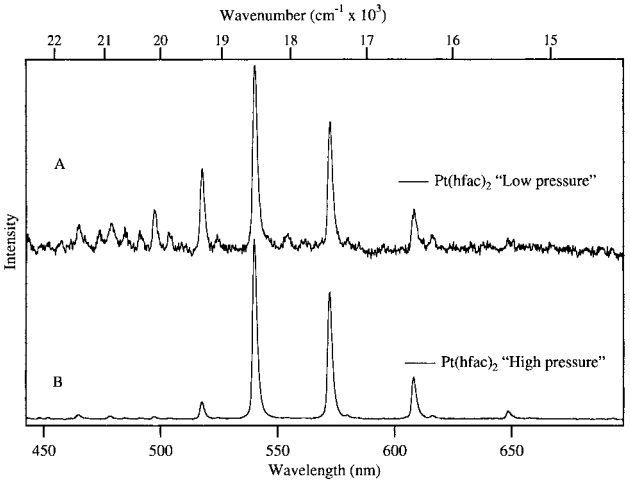

Figure 3. Emission spectra observed from 440 nm excitation of Pt-$(hfac)_2$. (a) Spectrum observed at a pressure of no greater than the vapor pressure of $Pt(hfac)_2$. (b) Spectrum observed using a static chamber with $Pt(hfac)_2$ at its vapor pressure with ~1 bar Ar buffer.

Most of the numerous features between 14 000 and 10 000 cm^{-1} correlate peak for peak with those observed in the gas cell experiment discussed above. Both the overall signal and the signal to noise ratios observed in the molecular beam are lower than those which were observed in the static gas cell. By 13 500 cm^{-1} the appearance of new bands and spectral congestion obscure the features previously observed in the cell spectrum.

At 13 950 cm^{-1} a new narrow band appears. This feature has a fwhm of approximately 250 cm^{-1}. When the band is viewed at the full resolution of the spectrum, what appears to be noise at first glance in Figure 2c is seen to actually be a multitude of sharp lines.[36] The spacing between these lines varies from 5 to 15 cm^{-1}.

In the visible region of the spectrum, a variety of sharp peaks similar to those observed in the cell experiment are observed with identical peak locations. In addition a variety of broader peaks are also observed. Numerous poorly resolved bands are observed between 17 500 and 15 500 cm^{-1}. Identification of clear progressions is difficult due to spectral congestion in this region. However a spacing of 600 cm^{-1} between several of the bands can be measured from the molecular beam spectrum. There is a new band system consisting of at least six peaks appearing at 19 000 cm^{-1}. The band system at 23 000 cm^{-1} that was identified in the gas cell spectra is clearly observable in the molecular beam spectra.

In the region around the laser excitation source at 308 nm a number of features are present. A sharp peak at 31 830 cm^{-1} is observed at slightly lower energy than the laser line. In addition, a shoulder is observed on the Rayleigh edge of the laser line at 31 940 cm^{-1}. At higher energy than the laser, a vibronic progression similar to that observed in the cell spectrum is observed. The features are separated by a spacing of approximately 650 cm^{-1} just as in the cell spectrum.

3. $Pt(hfac)_2$. Gas Cell Luminescence. Figure 3 displays the luminescence spectra obtained from $Pt(hfac)_2$ in the low-pressure gas cell. The spectrum consists of many features, all of which are observed under 308 nm excitation and 440 nm excitation.

(36) Hanna, S. D. Ph.D. Dissertation, UCLA, 1995; Chapter 4.

Table 2. Assignments of the Emission Bands of NiF Resulting from the Photolysis of $Ni(hfac)_2$

lower state energy	symmetry	upper state energy	symmetry	transition energy	observed
0	$^2\Pi_{3/2}$	23 504	$^2\Pi_{1/2}$	23 504	23 532
251	$^2\Pi_{1/2}$	23 504	$^2\Pi_{1/2}$	23 253	23 301
0	$^2\Pi_{3/2}$	22 954	$^2\Pi_{3/2}$	22 954	22 976
251	$^2\Pi_{1/2}$	22 954	$^2\Pi_{3/2}$	22 703	22 733
830	$^2\Delta_{5/2}$	22 954	$^2\Pi_{3/2}$	22 124	22 145
1574	$^2\Sigma$	23 504	$^2\Pi_{1/2}$	21 930	21 975
1574	$^2\Sigma$	22 954	$^2\Pi_{3/2}$	21 380	21 410
0	$^2\Pi_{3/2}$	19 983	$\Omega = {}^1/_2$	19 983	20 008
0	$^2\Pi_{3/2}$	19 719	$\Omega = {}^3/_2$	19 719	19 764
251	$^2\Pi_{1/2}$	19 719	$\Omega = {}^3/_2$	19 468	19 484
565	$\Omega = {}^3/_2$	19 719	$\Omega = {}^3/_2$	19 154	19 188
1574	$^2\Sigma$	19 719	$\Omega = {}^3/_2$	18 145	18 147
2224	$\Omega = {}^3/_2$	19 983	$\Omega = {}^1/_2$	17 759	17 756
2224	$\Omega = {}^3/_2$	19 719	$\Omega = {}^3/_2$	17 495	17 510

Under 440 nm excitation and low-pressure conditions (cell pressure less than or equal to the vapor pressure of the compound), the spectrum in Figure 3a is observed. In the visible region of the emission spectrum, a well-defined vibronic progression is observed. This feature is observed under both 440 and 308 nm excitation, and under the lower energy excitation, a higher signal to noise ratio is achieved. This band system has its origin at approximately 18 500 cm^{-1}. The peaks are clustered into well-defined groups proceeding to lower energy with the most intense members at 540, 572, 608, 649, and 694 nm. The spacing between each group of peaks is approximately 1050 cm^{-1}, while the spacing between individual adjacent peaks in a group is approximately 230 cm^{-1}. To higher energy from the origin there are many peaks in the region from 445 to 530 nm with prominent peaks at 517, 497, and 477 nm.

Effect of Inert Buffer Gas. Under "high"-pressure conditions with added Ar buffer gas to a total pressure of ~1 bar, similar spectra are observed as illustrated in Figure 3b. However, the peaks to high energy show reduced intensity as is apparent by comparing Figures 3a and 3b. In particular the bands between 445 and 530 nm show different relative intensities. Also, the smaller peaks in the main progression to lower energy show reduced intensity.

Discussion

1. Assignments from the $Ni(hfac)_2$ Spectra. Luminescence from Nickel Atoms. The intense sharp lines observed in both the gas cell spectrum and the molecular beam are assignable as nickel atomic lines. The bands marked with short vertical lines in Figure 1d are assigned to nickel atomic emission.[37,38] The majority of the new bands appearing in the molecular beam spectra are attributable to Ni atomic lines. Nickel atomic lines are observed under all conditions studied. The observation of nickel atomic lines under CVD conditions is not unexpected for $Ni(hfac)_2$. Their observation, however, does confirm that nickel atoms are produced in the gas phase due to laser photolysis.

Luminescence from Nickel Fluoride. The bands marked with triangles in Figure 1a are assigned as luminescence from NiF. The state assignments are summarized in Table 2. The bands due to NiF do not have well-resolved rotational band profiles beyond one case of a doubled band head at 451.6 nm. Because of this a rotational spectral simulation was not attempted. Similarly, the lack of observable vibrational bands and the corresponding lack of vibrational characterization of NiF prevents the analysis of the internal energies of the NiF photoproducts. Nevertheless, the observation of these states of NiF clearly demonstrates the presence of NiF and shows that metal fluoride production is not unique to copper in the photofragmentation of metal hfac compounds.

CH Luminescence. Emission from the CH diatomic molecule is labeled by diamonds in Figure 1b. The unambiguous assignment of CH comes not only from the band head positions but also from the rotational line spacing of ~28 cm^{-1} observable in the molecular beam spectra.[39] The presence of CH under both gas cell and collision-free molecular beam conditions implies that this product is generated directly from $Ni(hfac)_2$. The origin of this CH is therefore probably from the β carbon CH on the hfac moiety.

Unassigned Luminescence Bands. There are several bands which we are unable to assign as either a ligand fragment, atomic emission, or metal-containing fragment emission. In the low-pressure chamber, the bands at 371.0, 371.7, 387.1, 389.9, 399.1, 411.5, 422.2, 445.7, 448.1, 452.8, 461.2, 469.5, 475.0, 483.8, 486.1, 516.0, 532.8, 544.6, and 545.1 nm cannot be assigned.

In the molecular beam, of the new peaks that appear, only the ones at 397.1, 400.5, 447.0, 506.5, 508.0, 509.5, 511.4, and 514.5 nm cannot be assigned to Ni atomic emission. Because photolysis produces luminescent metal fluorides, and because NiF luminescence is prominent in the spectra, we speculate that these unassigned bands could be due to previously unobserved states of NiF. This gas-phase synthesis of metal fluorides may provide a unique opportunity for further study of metal fluorides in the gas phase.

2. Assignments from the $Cr(hfac)_3$ Spectra. Luminescence from Chromium Atoms. The intense sharp lines observed in both the gas cell spectrum and the molecular beam are assigned to atomic chromium emission. Chromium atomic lines are observed under all conditions studied. Their observation confirms that chromium atoms are produced in the gas phase due to laser photolysis.

Luminescence from Chromium Fluoride. The highly structured luminescence observed in the high-pressure gas cell centered at 850 nm under 343 nm excitations is assigned as the transition from the $A^6\Sigma$ excited state of CrF to the $X^6\Sigma$ ground state. Previous studies on chromium flux heated in the presence of F_2 or CaF revealed a similar spectrum.[34] The E_0 of this emission is reported to occur at 9624 cm^{-1}. The stretching frequency in the excited state is 581 cm^{-1}, while that of the ground state is 661 cm^{-1}. Hot bands through $\Delta n = -9$ are readily identifiable in the cell spectrum shown in Figure 2a. A summary of the observed features with vibronic assignments for the $A^6\Sigma \rightarrow X^6\Sigma$ transition of CrF is given in Table 1. To higher energy than the $\Delta n = -6$ band the structure begins to be washed out due to spectral congestion. The $B^6\Sigma$ state of CrF is at 16 864 cm^{-1} and may be contributing to the spectral congestion in this region. In the molecular beam under 308 nm excitation, the $A^6\Sigma \rightarrow X^6\Sigma$ emission is observed but not as strongly as in the cell under 343 nm excitation. This is explained by the fact that the $D^6\Sigma$ state of CrF absorbs strongly at 308 nm. Thus CrF produced in the molecular beam may be further fragmenting due to absorption at the excitation wavelength. The molecular beam produces molecules which are

(37) Wiese, W. L.; Martin, G. A. *Wavelength and Transition Probabilities for Atoms and Atomic Ions*; U.S. Government Printing Office: Washington, DC, 1980.

(38) Striganov, A. R.; Sventitskii, N. S. *Tables of Spectral Lines of Neutral and Ionized Atoms*; IFI/Plenum: New York, 1968.

(39) Pearse, R. W. B., Gaydon, A. G. *The Identification of Molecular Spectra*, 3rd ed.; Chapman and Hall: London, 1976.

Table 3. Observed Electronic States of CrF Resulting from the Photolysis of $Cr(hfac)_3$[33−35]

state	T_e	ω_e	$\omega_e x_e$	characteristic bands (cm^{-1})
$X^6\Sigma$	0	664		
$A^6\Sigma$	9 624	581	2	9 916, 10 490, 11 064
$B^6\Sigma$	16 864	605		16 864, 16 203, 16 137
?	23 154			23 154, 22 498, 21 814
D		∼600		31 777, 31 180, 30 051
?		650		34 123, 35 023, 35 700

colder initially and which would be expected to have slower rates of internal conversion. In addition the lack of collisions prevents relaxation to the lowest excited state ($A^6\Sigma$) of CrF. These factors all contribute to the molecular beam spectra being far richer in features and correspondingly more congested.

The $B^6\Sigma \rightarrow X^6\Sigma$ luminescence from CrF is clearly observed in the molecular beam spectrum. Identification of many of the hot bands is difficult due to spectral congestion in this region. The $B^6\Sigma \rightarrow X^6\Sigma$ state has an E_0 of 16 864 cm^{-1} and was reported previously. A vibrational frequency of approximately 605 cm^{-1} was also reported which matches well with the observed spacing of ∼600 cm^{-1}.

Bands observed in the blue region of the spectrum have a spacing characteristic of CrF. No electronic state for CrF in this region has been previously reported; however the characteristic spacing is a strong indication that this a previously unknown state of CrF. The E_0 appears to occur at 23 154 cm^{-1}, but spectral congestion could prevent identification of other bands. The 0,1 band occurs at 22 498 cm^{-1}. This gives rise to an ground state vibrational energy of 656 cm^{-1} which is within experimental error of the 664 cm^{-1} reported for the ground state vibrational frequency of CrF. Likewise the 0,3 band is observed at 21 814 cm^{-1}.

Three bands on the Rayleigh edge of the laser are observed at 31 777, 31 180, and 30 051 cm^{-1}. While there are not enough features to allow for conclusive identification, these bands occur in the region expected for the $D^6\Sigma \rightarrow X^6\Sigma$ transition of CrF.

Unassigned Luminescence. While many of the features observed in the gas phase luminescence and molecular beam spectra can be assigned, there are still many features that cannot be assigned. Many of these features are difficult to resolve due to spectral congestion or low signal to noise ratios. Others, such as the band systems centered at 37 000 and 13 950 cm^{-1}, are well resolved but have no literature precedent. The simplicity of these features suggests that they may be due to a diatomic species, perhaps CrF, CrC, or CrO, but no further assignment can be made. A summary of CrF band systems observed and suspected CrF band systems is in Table 3.

3. Assignments from the $Pt(hfac)_3$ Spectra. Luminescence from Platinum Carbide. All major luminescence features present in Figure 3 can be assigned to the $A \rightarrow X$ transition of PtC. There are no features present that we can assign to either Pt atoms or PtF. Unfortunately, there is no literature precedent for PtF luminescence; therefore, we cannot be certain that PtF is not present. It is possible that Pt atoms may be present in nonluminescent states. Spectral congestion in the hot band region from 445 to 530 nm may be obscuring some small features; however, all clearly identifiable peaks are assignable to PtC luminescence, as is clear from the calculation in Figure 4. The effect of inert buffer gas is attributable to collisional cooling of the PtC photofragment.

4. Mechanisms of Fragmentation for Metal hfac Compounds. Formation of MF and M. The emission of the diatomic metal fluorides CuF, NiF, and CrF occurs under the collision free conditions of the molecular beam. This observation implies that the formation of this photoproduct is most likely a unimolecular process. It is possible that clustering occurs in the molecular beam due to the cold temperature and that such clusters could provide direct interactions between otherwise nonbonded metal complexes. However, we also observe the metal fluorides in high-temperature gas phase experiments. Therefore we conclude that the appearance MF in collision free conditions is due to an intramolecular process and not a polymolecular complex.

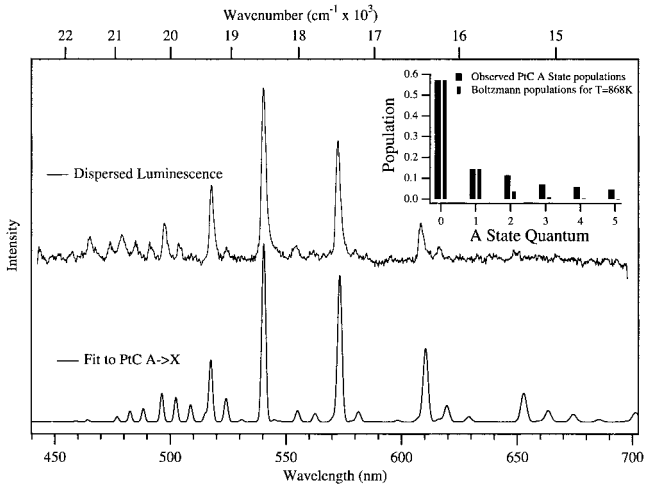

Figure 4. Calculated low-pressure emission spectrum of PtC. The insert shows the vibrational populations used in the calculation and the Boltzmann populations for $T = 868$ K.

The metal-containing diatomic fragments are not formed by generation of a plasma followed by recombination of atoms or ions. A plasma would produce metal ions; we only observe emission from neutral metal atoms in both the evacuated gas cell experiments and the molecular beam experiments. A recombination mechanism cannot explain the specificity of our observations of MF formation from Cu, Ni, and Cr hexafluoroacetonate complexes and PtC from the Pt hexafluoroacetonate complex. A nonspecific physical (as opposed to chemical) mechanism such as plasma formation would be expected to produce many different metal-containing diatomics including metal oxides; we do not see species such as CrO or NiO. Finally, the results of the experiments in the supersonic expansion molecular beam, where there are no collisions, show that metal fluorides do not arise from a plasma. Therefore we conclude that the appearance of MF under the beam conditions does not result from a plasma, and that the appearance of MF and MC in the gas cell is not dominated by the cooling phase of a plasma. Rather, an intramolecular chemical mechanism must be dominant.

The production of metal monofluorides requires that a large amount of internal motion occur in the molecule such that the fluorine may come in contact with the metal. We propose that intramolecular fluorine atom abstraction by the metal might occur by either or both of two simple mechanisms. The first mechanism involves metal migration as illustrated in the bottom pathway in Figure 5. Alternate binding modes of metals to β-diketonates are known,[40−42] particularly for platinum,[40,41] including binding through the π system (η^3) of the acetylacetonyl moiety or binding in a sigma manner (η^1) to the β carbon of the acetylacetonyl moiety. If the metal migrates onto the π system or is bound through the β carbon, it is much closer to

(40) Behnke, G. T.; Nakamoto, K. *Inorg. Chem.* **1967**, *6*, 440.
(41) Lewis, F. D.; Miller, A. M.; Salvi, G. D. *Inorg. Chem.* **1995**, *34*, 3173.
(42) Kimiya, S.; Kochi, J. K. *J. Am. Chem. Soc.* **1977**, *99*, 11.

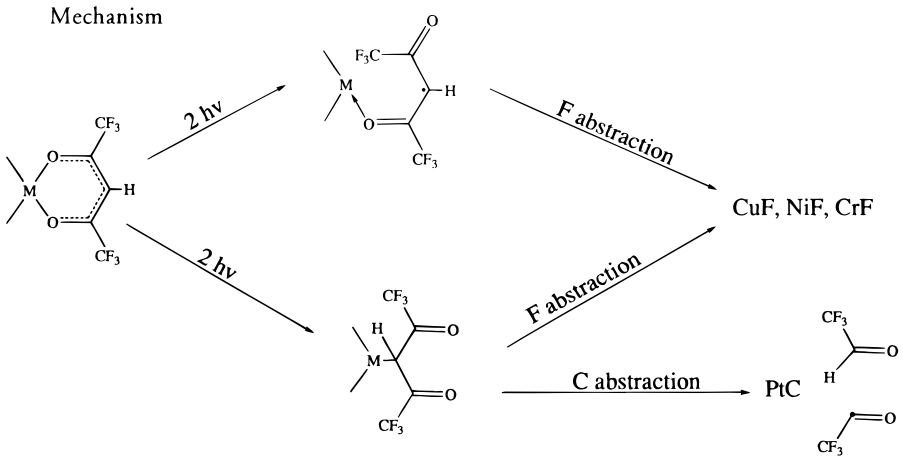

Figure 5. Proposed intramolecular rearrangements that explain the observed photofragmentation patterns of the metal−hfac compounds studied.

the fluorines on the CF_3 groups than it would be in the standard bidentate binding mode. This mechanism is discussed in more detail in the following section.

A second mechanism which seems more likely for Cu, Ni, and Cr is illustrated in the top pathway in Figure 5. The single photon absorption at 308 nm has been assigned as a $\pi \rightarrow \pi^*$ ligand-centered transition.[43,44] One photon excites the $\pi \rightarrow \pi^*$ system on the ligand and another photon excites an LMCT, breaking a M−O bond. The resulting half-free ligand is bound through one oxygen. The unbound side can then rotate about the (now) formally C−C single bond, placing the CF_3 group in direct contact with the metal. The metal abstracts the fluorine, and the resulting MF chemiluminesces. This mechanism involves the least motion of the atoms in the molecule. If a collision occurs before the abstraction takes place, free copper can be produced. However, this collision is not required for production of luminescent Ni or Cr.

The production of luminescent metal atoms may arise directly from the $M(hfac)_n$ fragmentation process, or it may be a result of absorption of the excitation laser light by either atoms in nonluminescent states or by MF which then fragments to produce M* + F. One note on that regard is that laser-induced fluorescence excitation spectra of $Cr(hfac)_3$ show atomic line resonances at 373.08 and 373.20 nm from ground state Cr.[45] This result indicates that Cr atoms are being produced in the ground state upon multiphoton fragmentation of the $Cr(hfac)_3$ molecule.

Formation of PtC. Perhaps the most intriguing and unexpected result of these studies is that of the platinum carbide production. In our original copper hfac paper we raised the possibility that an alternative binding mode, a metal−carbon η^1 bond that has been observed for $Pt(hfac)_2$, was involved in the photofragmentation mechanism.[1] The data and calculations discussed below prove that PtC is an important photofragmentation product.

The observed emission spectrum in Figure 3 is in excellent agreement with the known A → X emission of PtC. A fit to the spectrum was obtained by using literature values[26,27] for diatomic molecular parameters to calculate the excited and ground state vibrational energy levels. The vibrational line strengths were calculated using wave packet propagation and the time dependent theory of electronic spectroscopy. Figure 4 shows the fit to the low-pressure spectrum of the A → X transition of PtC. The adjustable parameters were the populations of vibrational levels in the excited states. The vibrational state populations are shown as the insert in Figure 4. The parameters used for the fits to the various states of PtC are summarized in Table 4.

Table 4. Spectroscopic Parameters Used in the Intensity Fits To Determine the Vibrational and Rotational Temperatures of PtC[45]

state	T_e	ω_e	$\omega_e x_e$	T_{vib}
X	0	1051.18	4.87	
A	18 510	818.8	5.5	868

Boltzmann fits to the vibrational populations from the luminescence studies were carried out to determine the vibrational temperature of PtC. The fit shows that the ejected PtC is vibrationally hot with a calculated temperature on the order of 1000 K. The ratio of the A state $v = 0$ population to the $v = 1$ population implies a temperature of 870 K. However, the populations of the $v = 2, 3, 4, 5$ states are much higher than predicted for a Boltzmann population at this temperature. Selective population of the higher levels may occur. The PtC fragment produced from the $Pt(hfac)_2$ photofragmentation is vibrationally hot, as is the case for CuF from $Cu(hfac)_2$. The vibrational "temperature" is substantially lower than those observed for CuF (~1700 K). The amount of energy disposed of in electronic and vibrational excitation of the PtC fragment is approximately 30 000 cm^{-1}.

The alternative η^1 binding mode that is specifically known for β-diketonate complexes of platinum is important in the production of PtC. It is a simple matter to eliminate relatively stable fragments from an already PtC-bonded species to produce the final PtC diatomic as shown in Figure 5. It cannot be ruled out that binding through the β carbon of the acetylacetonyl moiety could be involved in the mechanism for the production of metal fluorides. The different patterns (carbides versus fluorides) observed in different metals could be due to the differences in metal binding strength to the β carbon. Platinum may bind particularly well to the β carbon, which would explain why this intermediate has been identified previously. The production of PtC has a large driving force; the bond strength of PtC is 50 830 cm^{-1} (145.3 kcal/mol).[46] This strong metal carbon bond may substantially weaken the carbon−carbon bonds, which results in the mechanism which produces PtC. However, if the metal−β carbon bond is weak, then perhaps fluorine abstraction could dominate.

(43) Wexler, D.; Zink, J. I. *Inorg. Chem.* **1996**, *35*, 4064.
(44) Fackler, J. P.; Cotton, F. A.; Barnum, D. W. *Inorg. Chem.* **1963**, *2*, 97.
(45) D. S. Talaga. Unpublished work.
(46) *Données Spectroscopiques Relatives aux Molécules Diatomiques*, 17th ed.; Rosen, B., Ed.; Pergamon Press, Inc: New York, 1970; pp 515.

Conclusions

Bare metal atoms and diatomic metal fluorides are common photofragments from metal hfac compounds. The spectroscopic studies of UV photofragmentation of $M(hfac)_n$ under a range of gas phase conditions with no surface interactions imply that MF is formed by intramolecular fluorine abstraction by the metal. The MF molecule is both rotationally and vibrationally hot ($T \sim 1700$ K). Although the one-photon transition in the $M(hfac)_n$ complexes at 308 nm has been assigned as ligand-centered $\pi \rightarrow \pi^*$, there is likely some metal contribution to the orbitals involved in the multiphoton transition. Collisions are required for luminescent metal production from $Cu(hfac)_2$ but not from $Cr(hfac)_3$ or $Ni(hfac)_2$.

The production of PtC as a luminescent photofragment from $Pt(hfac)_2$ implies that the type of coordination of the ligand to the metal is very important in determining the photoproduct observed spectroscopically. $Pt(hfac)_2$ is known to bind to the β carbon of the ligand, and Pt is the only metal for which metal carbide luminescence during photofragmentation is observed.

The spectra from the Ni and Cr compounds contain many atomic lines in addition to the metal fluoride bands. In our earlier study of $Cu(hfac)_2$ atomic lines were observed in the presence of collisions but copper fluoride was found in the absence of collisions. Collisions are not necessary for atomic metal emission in the cases of $Ni(hfac)_2$ and $Cr(hfac)_3$.

Materials deposited by the laser photochemistry of these complexes would be expected to show impurities. Photochemically derived deposits of metals from $Cu(hfac)_2$, $Cr(hfac)_3$, or $Ni(hfac)_2$ are expected to show fluorine incorporation due to the gas phase component of the deposition process. Similarly the photochemical production of platinum metal from $Pt(hfac)_2$ is expected to show carbon contamination[6] because of the production of PtC in the gas phase portion of the deposition process. In all cases, however, the contributions of surface reactions will also be important.

Acknowledgment. This work was supported by a grant from the National Science Foundation (CHE-9509275).

IC971340X